NLRX1 dampens oxidative stress and apoptosis in tissue injury via control of mitochondrial activity

Geurt Stokman,[1] Lotte Kors,[1]* Pieter J. Bakker,[1]* Elena Rampanelli,[1] Nike Claessen,[1] Gwendoline J.D. Teske,[1] Loes Butter,[1] Harmen van Andel,[1] Marius A. van den Bergh Weerman,[1] Per W.B. Larsen,[1] Mark C. Dessing,[1] Coert J. Zuurbier,[2] Stephen E. Girardin,[3] Sandrine Florquin,[1] and Jaklien C. Leemans[1]

[1]Department of Pathology and [2]Department of Anaesthesiology, Academic Medical Center, Amsterdam, Netherlands
[3]Department of Laboratory Medicine and Pathobiology, University of Toronto, Toronto, ON, Canada

Mitochondrial dysfunction is the most prominent source of oxidative stress in acute and chronic kidney disease. NLRX1 is a receptor of the innate immune system that is ubiquitously expressed and localized in mitochondria. We investigated whether NLRX1 may act at the interface of metabolism and innate immunity in a model of oxidative stress. Using a chimeric mouse model for renal ischemia–reperfusion injury, we found that NLRX1 protects against mortality, mitochondrial damage, and epithelial cell apoptosis in an oxidative stress–dependent fashion. We found that NLRX1 regulates oxidative phosphorylation and cell integrity, whereas loss of NLRX1 results in increased oxygen consumption, oxidative stress, and subsequently apoptosis in epithelial cells during ischemia–reperfusion injury. In line, we found that NLRX1 expression in human kidneys decreased during acute renal ischemic injury and acute cellular rejection. Although first implicated in immune regulation, we propose that NLRX1 function extends to the control of mitochondrial activity and prevention of oxidative stress and apoptosis in tissue injury.

INTRODUCTION

TLRs and NOD-like receptors (NLRs; also known as nucleotide-binding, lots of leucine-rich repeats-containing protein members) are important regulators of innate immunity during pathogen infection and sterile tissue injury (Kopp and Medzhitov, 1999; Martinon et al., 2002; Leemans et al., 2014). We have previously found that TLR2, TLR4, and NLRP3 are critically involved in the control of inflammation, tubular epithelial cell (TEC) injury, and tubulointerstitial fibrosis in animal models of acute and chronic kidney injury (Leemans et al., 2005, 2009; Pulskens et al., 2008, 2010; Iyer et al., 2009). In sterile tissue injury, TLRs and NLRs are activated by damage-associated molecular patterns and subsequently mediate production and inflammasome-dependent processing of proinflammatory cytokines by caspase-1 (Leemans et al., 2014).

In contrast, NLRX1 has anti-inflammatory effects by negatively regulating antiviral immune responses in an inflammasome-independent fashion (Moore et al., 2008) and affects canonical NF-κB signaling via inhibition of TRAF6 binding to IκB kinase (Xia et al., 2011). A unique feature of NLRX1 is its localization at the mitochondrial matrix mediated by an N-terminal addressing sequence (Arnoult et al., 2009). Other studies show a role for NLRX1 in regulating cell death, either by affecting susceptibility of tumor cells to extrinsic apoptosis (Soares et al., 2014; Singh et al., 2015) or by regulating neuronal apoptosis through control of mitochondrial dynamics (Imbeault et al., 2014). These studies suggest a potential role of NLRX1 in mitochondrial control of apoptotic cell death, but no underlying mechanism was further investigated.

NLRX1 lacks both a pyrin and a caspase activation and recruitment domain, which are required for caspase-1 activation, either directly or through the adaptor ASC (Allen, 2014). Several mitochondrial proteins, including mitochondrial antiviral signaling protein (Moore et al., 2008), dynamin-related protein 1 (DRP1; Imbeault et al., 2014), and ubiquinol-cytochrome *c* reductase core protein II (UQCRC2; also known as cytochrome b-c1 complex subunit 2, mitochondrial; Arnoult et al., 2009), have been found to associate with NLRX1 and may be involved in inflammasome-independent, noncanonical NLR signaling. Of these, UQCRC2 provides an interesting connection to mitochondrial function, because gene mutations lead to mitochondrial complex III deficiency nuclear type 5, which is characterized by recurrent metabolic decompensation and involves a 50% decrease in complex III activity (Miyake et al., 2013).

*L. Kors and P.J. Bakker contributed equally to this paper.

Correspondence to Geurt Stokman: g.stokman@amc.uva.nl

Abbreviations used: ACR, acute cellular rejection; AKI, acute kidney injury; ATN, acute tubular necrosis; CsA, cyclosporine A; DHA, docosahexaenoic acid; IM-PTEC, immortalized mouse proximal tubular epithelial cell; IRI, ischemia-reperfusion injury; LDH, lactate dehydrogenase; NLR, NOD-like receptor; OCR, oxygen consumption rate; OXPHOS, oxidative phosphorylation; RNS, reactive nitrogen species; ROS, reactive oxygen species; TEC, tubular epithelial cell.

The Rockefeller University Press
J. Exp. Med. 2017 Vol. 214 No. 8 2405–2420
https://doi.org/10.1084/jem.20161031

Mitochondria have been reappraised as critical mediators of acute kidney injury (AKI; Ishimoto and Inagi, 2016). Mitochondrial dysfunction, and production of reactive oxygen and nitrogen species (ROS and RNS, respectively) occur in TECs during reperfusion, supposedly as a direct consequence of ATP depletion during ischemia (Devarajan, 2006). ROS- and RNS-induced modifications of proteins, lipids, or DNA result in disruption of cellular homeostasis and, together with mitochondrial cytochrome *c* release, in apoptosis (Ott et al., 2007). This, combined with a potential role for NLRX1 in mitochondrial-mediated cell death, prompted us to investigate if NLRX1 is involved in the pathogenesis associated with renal ischemia-reperfusion injury (IRI), the most common form of AKI in hospitalized patients (Susantitaphong et al., 2013).

In the present study we demonstrate that loss of NLRX1 significantly increased accumulation of ROS in both animal and cell models for IRI. Loss of NLRX1 was associated with an increased rate of oxidative phosphorylation (OXPHOS) compared with controls. NLRX1 KO cells underwent oxidant-dependent apoptosis, which could be blocked by inhibiting UQCRC2 expression. Our data suggest that NLRX1 is a regulator of mitochondrial function, which controls OXPHOS and prevents excessive ROS formation during IRI, thereby preventing apoptosis of TECs.

RESULTS

Loss of NLRX1 increases tubular epithelial apoptosis during renal IRI

We examined the role of NLRX1 in renal IRI using WT and *Nlrx1* KO mice. To induce AKI, one renal artery was clamped for 30 min, followed by a 1- or 5-d reperfusion phase. In WT animals, *Nlrx1* transcription was reduced at day 1 after ischemia but returned to baseline transcription at day 5 (Fig. 1 A). Punctate expression of NLRX1 protein was most prominent in proximal TECs, characterized by an F actin–rich brush border (Fig. 1 B), but absent from glomerular cells, capillary endothelium, and collecting ducts (not depicted). During IRI, labeling for NLRX1 was predominantly present in detached epithelial cells and sporadically in interstitial cells (Fig. 1 B). We found that *Nlrx1* transcription is present in cultured TECs and inflammatory cells, including different macrophage subsets and granulocytes (Fig. 1 C). At day 1 of reperfusion, we found no difference in the degree of tubular necrosis in the corticomedullary region of ischemic kidneys from WT and *Nlrx1* KO mice but a significantly higher degree of tubular necrosis in *Nlrx1* KO mice at day 5 after ischemia (Fig. 1 D). This was further reflected by plasma lactate dehydrogenase (LDH) levels (Fig. 1 E). In contrast, tubular epithelial apoptosis was significantly increased at both days 1 and 5 after ischemia in *Nlrx1* KO mice compared with WT controls (Fig. 1 F).

Next we examined the influx of inflammatory cells in renal tissue during IRI. We did not observe a difference in granulocyte (Fig. 1 G) and macrophage accumulation (Fig. 1 I) between WT and *Nlrx1* KO animals during IRI except for a modest increase in the number of macrophages at day 5 after ischemia in the kidneys of *Nlrx1* KO mice. Interestingly, expression of CXCL1 (Fig. 1 H) and CCL2 (Fig. 1 J), important chemokines for neutrophil and macrophage migration to the ischemic kidney, respectively, were significantly increased in kidneys from KO compared with WT animals.

To determine renal function, we induced bilateral IRI by clamping both renal arteries to induce ischemia. We found that plasma creatinine was significantly increased in *Nlrx1* KO mice at day 1 after ischemia (Fig. 1 K). Whereas all WT animals survived until day 5, out of eight KO animals, five died before day 5 (Fig. 1 L); therefore, we did not include this time point in the analysis of renal function.

To further differentiate between the involvement of renal and leukocyte NLRX1 expression in IRI, we performed a series of BM transplantations to generate chimeric mice. To investigate the involvement of NLRX1 expression by leukocytes, we transplanted WT BM into *Nlrx1* KO recipients (WT → KO). To determine the relevance of renal NLRX1 expression, BM from *Nlrx1* KO mice was transplanted into WT recipients (KO → WT). As a control, WT recipients received BM from WT littermates (WT → WT). Transplantation efficiency was determined by flow cytometric analysis of CD45.1 and CD45.2 expression for WT and *Nlrx1* KO leukocytes, respectively (not depicted). BM chimeras with >75% donor-derived leukocytes were included for further analysis.

We induced bilateral renal IRI in the chimeras and sacrificed animals at day 1 of reperfusion, without any premature deaths occurring. In all groups, tubular damage was severe at this time point and extended from the corticomedullary area into the renal cortex. Cortical tubular epithelial necrosis (Fig. 1 M), plasma LDH levels (Fig. 1 N), and tubular apoptosis (Fig. 1 O) were all increased in WT → KO animals compared with WT → WT controls. Although KO → WT animals showed a strong trend toward increased tubular necrosis and LDH levels compared with WT → WT controls, tubular epithelial apoptosis was not as pronounced as in the WT → KO animals. Combined, these data show that in contrast to tubular apoptosis, the degree of tubular necrosis appears to be less affected by expression of epithelial NLRX1. We also found that inflammatory cell influx did not differ between WT and NLRX1 KO animals, with the exception of a small increase in F4/80 macrophages in NLRX1 KO animals at day 5 after IRI. The increase in TEC apoptosis in the absence of epithelial NLRX1 is thus the most striking feature during renal IRI. We therefore continued to examine the mechanism behind this.

Loss of NLRX1 promotes tubular oxidative stress during IRI

To examine how TECs from *Nlrx1* KO animals were more susceptible to apoptosis during renal IRI than WT animals, we performed stainings for 4-hydroxynonenal (Fig. 2 A) and nitrosylated tyrosine (Fig. 2 B) to indicate lipid peroxidation and protein nitrosylation, respectively. Tubular epithelial la-

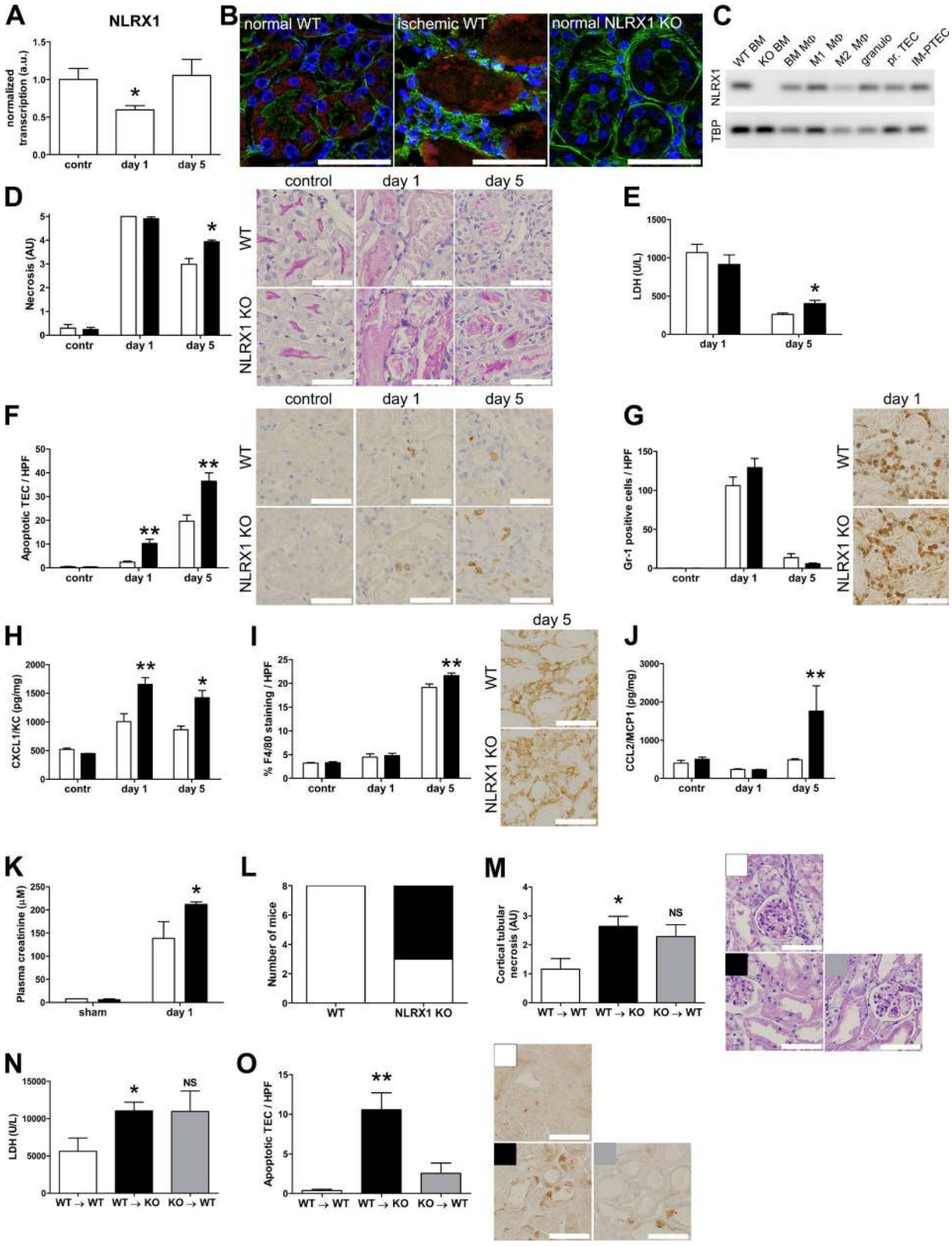

Figure 1. **NLRX1 deficiency increases tubular apoptosis during IRI.** (A) Transcription analysis of NLRX1 in kidneys from WT animals obtained the indicated time points during IRI ($n = 5$ per time point). (B) Confocal microscopic imaging of kidney tissue from respectively control WT, ischemic (day 1) WT, and NLRX1 KO mice stained for NLRX1 (red), F actin (green) and nuclei (blue). (C) Agarose gel electrophoresis for NLRX1 transcription of WT and KO BM,

beling was dramatically increased in kidneys from *Nlrx1* KO animals at day 1 after ischemia compared with WT controls, suggesting increased mitochondrial ROS and RNS production in these animals.

We next performed high-resolution transmission electron microscopy on tissue sections to examine mitochondrial morphology and fragmentation (Knott et al., 2008). We did not observe differences in mitochondrial morphology between TECs of normal WT and KO mice (Fig. 2, C and D). Kidneys from WT animals showed limited mitochondrial fragmentation in proximal epithelial cells at day 1 after ischemia (Fig. 2 E), whereas mitochondria from *Nlrx1* KO (Fig. 2 F) animals showed increased mitochondrial damage (Fig. 2 G) and the sporadic presence of a phagosome-like structure containing mitochondria (Fig. 2 H).

Transcription of glutathione peroxidase 1 and 3 were significantly increased in *Nlrx1* KO mice, whereas peroxiredoxin 1 and superoxide dismutase 2 were not different between WT and *Nlrx1* KO animals (Fig. 2 I). This suggests that decreased transcription of detoxification enzymes is not the cause of increased oxidative stress in KO mice. These data show that NLRX1 deficiency during renal IRI promotes mitochondrial dysfunction and radical production, which may underlie the increase in tubular epithelial apoptosis.

NLRX1 deficiency increases apoptosis dependent on mitochondrial oxygen radical production

To further examine the mechanism by which loss of NLRX1 affects oxidative stress, we isolated primary TECs from kidneys of WT and *Nlrx1* KO mice. Cells were exposed to hypoxia for 60 min by submersion under a layer of paraffin oil (Stokman et al., 2011), followed by 45 min of reoxygenation in medium. Mitochondrial superoxide accumulation was determined by MitoSOX Red. Accumulation of superoxide was significantly increased in primary TECs from *Nlrx1* KO mice after hypoxia, whereas TECs from WT mice appeared more resistant (Fig. 3 A). A 24-h duration of reoxygenation resulted in a significant increase in cleaved caspase-3 in cells from both WT and *Nlrx1* KO mice compared with normoxic controls (Fig. 3 B).

Renal IRI results in severe proximal tubule damage, whereas other nephron segments are less susceptible (Bonventre and Yang, 2011). Because primary cultures contain epithelial cells from all nephron segments and contaminating interstitial fibroblasts, we continued using the conditionally immortalized proximal tubular epithelial immortalized mouse proximal TEC (IM-PTEC) cell line (Stokman et al., 2010), which expresses NLRX1 (Fig. 3 C). We generated NLRX1 KO cells (cNLRX1), and control cells were transfected with the empty vector only (cEmpty; Fig. 3 C). Interestingly, superoxide accumulation was already increased in cNLRX1 cells under normoxic conditions (Fig. 3 D). Reoxygenation after hypoxia significantly increased superoxide accumulation in cNLRX1 cells compared with both normoxic controls and cEmpty cells exposed to reoxygenation (Fig. 3, D and G). Similarly, we found that caspase-3 cleavage was increased after hypoxia in cNLRX1 cells compared with cEmpty controls (Fig. 3, E and H). In line, culture in a hypoxia chamber for 48 h increased caspase-3 cleavage in cNLRX1 cells compared with cEmpty controls (Fig. 3, F and I). Exposure to the superoxide dismutase-inhibiting compound diethyldithiocarbamate or the glutathione-depleting agent diethyl maleate resulted in increased superoxide accumulation in cNLRX1 cells compared with cEmpty controls (Fig. 3, J and K). These data confirm that loss of NLRX1 is associated with increased oxidative stress and apoptotic cell death after hypoxic cell stress.

To examine the role of oxidative stress in the regulation of apoptosis in NLRX1-deficient cells, we incubated cells with N-acetyl cysteine, MitoTEMPO, and resveratrol for 24 h after hypoxia. Antioxidant treatment decreased apoptosis of cNLRX1 cells to a degree similar as cNLRX1 cells maintained at normoxic conditions (Fig. 4 A). Treatment with cyclosporine A (CsA), an inhibitor of the mitochondrial permeability transition pore, also reduced apoptosis compared with normoxic controls (Fig. 4 B). In contrast, treatment with TNF did not enhance susceptibility to apoptosis in cNLRX1 cells (Fig. 4 B). Compared with normoxic controls, resveratrol and CsA prevented increased LDH levels

total BM-derived macrophages (Mφ), and ex vivo differentiated M1 and M2 Mφ, granulocytes, primary cultured TECs and the proximal tubular epithelial IM-PTEC cell line, amplicon sizes: NLRX1, 90 bp and TBP, 89 bp. (D–J) Analysis of unilateral IRI outcome in WT mice (white bars, $n = 8$ per time point) and NLRX1 KO mice (black bars, $n = 8$ per time point). (D) Semiquantitative histological scoring of tubular necrosis of kidney sections; representative periodic acid-Schiff with digestion images are shown. (E) Plasma LDH levels expressed in units per liter. Immunohistochemistry was performed on kidney sections for (F) cleaved caspase-3, (G) Gr-1, and (I) F4/80; representative images are shown for each staining. Positive (F) TECs or (G) Gr-1 expressing cells were counted per high-power field (HPF), and (I) F4/80 expressing cells were quantified by digital image analysis and expressed as percentage positive staining per HPF. ELISA was performed on kidney homogenates for (H) CXCL1 and (J) CCL2. Chemokine levels are corrected for total protein contents of the homogenates. (K) Analysis of bilateral IRI outcome in WT mice (white bars, $n = 2$ in sham group, $n = 8$ in IRI group) and NLRX1 KO mice (black bars, $n = 2$ in sham group, $n = 8$ in IRI group). Plasma creatinine levels of mice subjected to bilateral injury and sacrificed at day 1. (L) Survival of WT ($n = 8$) and NLRX1 KO ($n = 8$) mice at day 5 after bilateral ischemia; white area represents live animals, black area represents dead animals. (M–O) Analysis of bilateral IRI outcome in BM chimeric animals: WT BM into WT recipients (WT → WT, white bars, $n = 7$), WT BM into KO recipients (WT → KO, black bars, $n = 7$), and KO BM into WT recipients (KO → WT, gray bars, $n = 7$). Analysis of (M) semiquantitative histological scoring of tubular necrosis of kidney sections, (N) plasma LDH levels, and (O) immunohistochemical detection of cleaved caspase-3 stained TECs per HPF. Bars, 50 µm (B); 100 µm (D, F, G, I, M, and O). All data are expressed as mean ± SEM and were analyzed using a Mann-Whitney *U* test (*, $P < 0.05$; **, $P < 0.01$). a.u., arbitrary units; contr, contralateral kidney; NS, not significant.

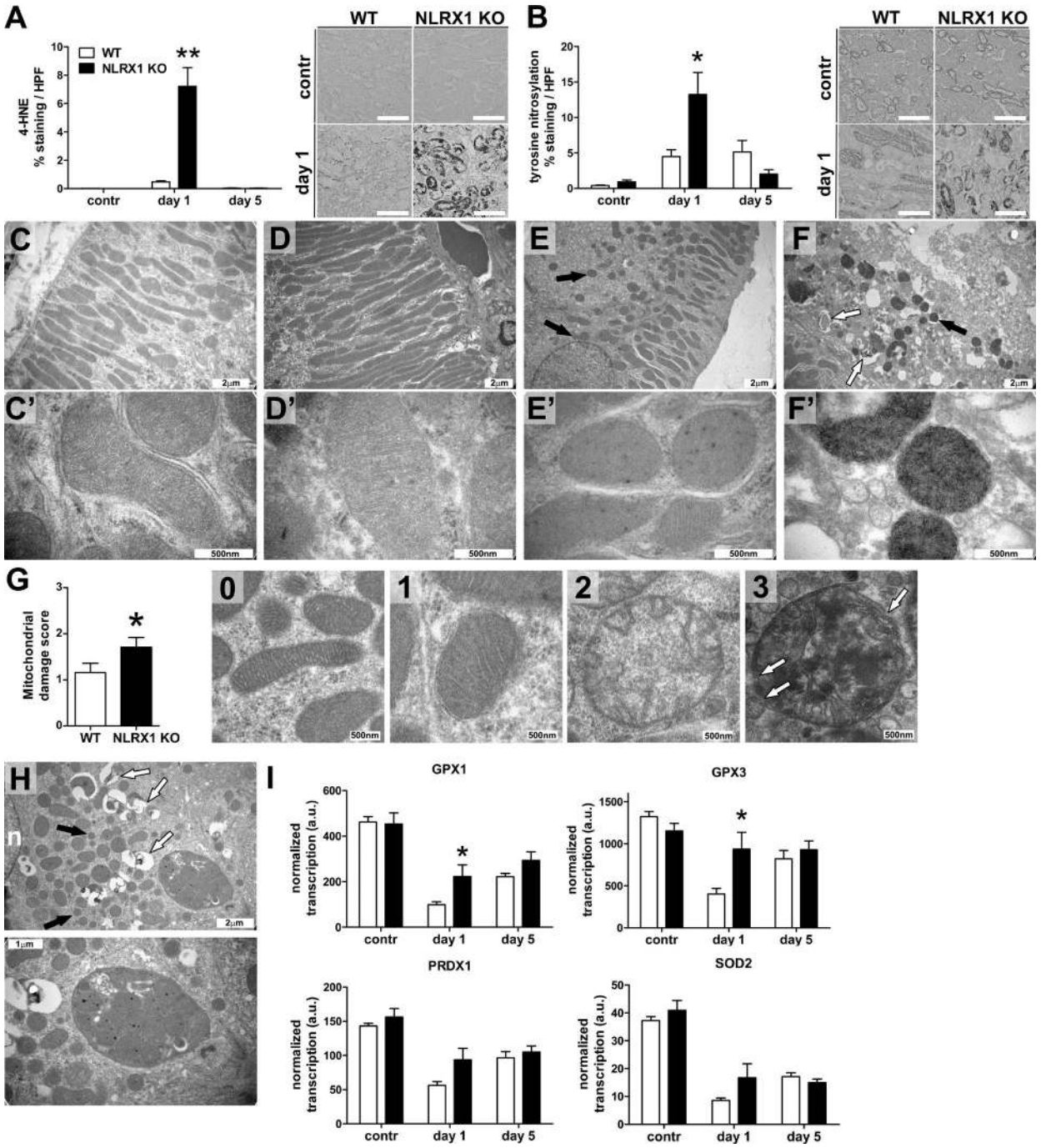

Figure 2. **Increased oxidative stress and disturbed mitochondrial morphology in NLRX1 KO mice during IRI.** Digital image analysis of immunohistochemistry for (A) 4-hydroxynonenal (4-HNE) and (B) nitrosylated tyrosine on kidney tissue sections from WT and KO animals (white and black bars, respectively, $n = 8$ per group) at the indicated time points during IRI (left). Representative images are presented right for each stain. Bars, 100 µm. All data are expressed as mean ± SEM and were analyzed using a Mann-Whitney *U* test (*, $P < 0.05$; **, $P < 0.01$). contr, contralateral kidney. (C–F) Transmission electron microscopic imaging of kidney sections obtained from (C and E) WT and (D and F) NLRX1 KO animals. Proximal tubules in contralateral kidneys from (C) WT and (D) NLRX1 KO animals show normal mitochondrial morphology. (E) Kidney section from a WT animal at day 1 after ischemia shows mild mitochondrial fragmentation (indicated by black arrows). (F) Kidney section from an NLRX1 KO animal at day 1 after ischemia shows extensive mitochondrial fragmentation (indicated by black arrow) and mitochondrial collapse (indicated by white arrows). Bars, 2 µm. (C′–F′) High-magnification imaging of mitochondria from (C′ and D′) contralateral kidneys and (E′ and F′) injured kidneys. (G) Semiquantitative scoring of mitochondrial damage in WT and NLRX1 KO mice at day 1 during IRI (white and black bars, respectively, $n = 3$ per group). Examples of each score are presented. Data are expressed as mean ± SEM and were analyzed using a Mann-Whitney *U* test (*, $P < 0.05$). White arrows indicate sites of membrane rupture. (H) Transmission electron microscopic

during reoxygenation of cNLRX1 cells but not of cEmpty cells (Fig. 4 C). These findings confirm that increased apoptosis in NLRX1 KO cells results from mitochondrial damage and oxidative stress.

NLRX1-deficient cells show mitochondrial morphological abnormalities with normal enzyme function

Mitochondrial morphology changes during reoxygenation were examined by labeling cells with the mitochondrial dye MitoTracker followed by confocal microscopy (Fig. 5 A). During normoxic conditions, cEmpty control cells (Fig. 5 A, top) showed a normal mitochondrial network, which was fragmented under hypoxic conditions. Upon reoxygenation, mitochondrial fusion led to a restored network. Interestingly, cNLRX1 cells (Fig. 5 A, bottom) showed a more diffuse labeling for mitochondria under normoxic conditions, followed by severe fragmentation during hypoxia. Reoxygenation showed a delayed recovery.

These findings were substantiated by analysis of the mitochondrial permeability transition pore using JC-1 (Fig. 5 B), in which we observed a decreased mitochondrial membrane potential in normoxic cNLRX1 cells compared with cEmpty controls. Reoxygenation in cNLRX1 cells was also accompanied by delayed recovery to normal membrane potential as under normoxic conditions when compared with cEmpty cells.

Loss of NLRX1 increases OXPHOS activity

NLRX1 was shown to interact with UQCRC2, a subunit of the mitochondrial complex III (Arnoult et al., 2009; Rebsamen et al., 2011). Because our data suggest that loss of NLRX1 primarily exacerbates mitochondrial dysfunction during hypoxic cell stress, we examined if NLRX1 deficiency affects OXPHOS. We examined the mitochondrial oxygen consumption rate (OCR) using a Seahorse Bioanalyzer. We found that under normoxic conditions, the OCR of cNLRX1 cells was significantly increased compared with cEmpty controls, specifically basal respiration, ATP production, and maximal respiration (Fig. 5, C and D). The extracellular acidification rate, which reflects glycolytic activity in cells, showed an inverse correlation to the OCR in cNLRX1 cells (Fig. 5 E). We confirmed increased complex II/III activity in vivo by examining cytochrome *c* reduction in isolated renal mitochondria from WT and NLRX1 KO mice (Fig. 5 F). We examined if metabolic enzyme activity was affected in NLRX1-deficient cells. Activity of citrate synthase, hexokinase, LDH, and short-chain-3-hydroxyacyl-CoA dehydrogenase were not significantly different in cEmpty and cNLRX1 cells (Fig. 5 G), indicating that loss of NLRX1 does not alter baseline enzyme activity. These data show that in NLRX1-deficient cells, OXPHOS is increased and glycolysis slightly decreased compared with controls, independent of upstream metabolic enzyme activity.

Interestingly, ATP levels in cNLRX1 cells were significantly decreased under normoxic conditions or during reoxygenation compared with cEmpty cells (Fig. 5 H). This suggests that although oxygen consumption and mitochondrial activity are increased in cNLRX1 cells, ATP consumption is likewise increased, or alternatively, ATP synthesis may be more inefficient compared with controls.

Knockdown of UQCRC2 or exposure to polyunsaturated fatty acid prevents apoptosis in cNLRX1 cells

Inactivating mutations in the *UQCRC2* gene reduces complex III activation in humans (Miyake et al., 2013). Because NLRX1 has been shown to associate with UQCRC2 (Arnoult et al., 2009; Rebsamen et al., 2011), we investigated if UQCRC2 is responsible for increased apoptosis of cNLRX1 cells after hypoxia. We treated both cEmpty and cNLRX1 cells with siRNA specific for UQCRC2 (Fig. 6 A) and subjected these cells to hypoxia followed by reoxygenation. As a control, both cell lines were treated with siRNA to GFP. Treatment of cNLRX1 cells with siRNA for UQCRC2 significantly reduced apoptosis compared with cells transfected with siRNA to GFP (Fig. 6 B). Knockdown of UQCRC2 prevented increased mitochondrial ROS during reoxygenation in both cEmpty and cNLRX1 cells (Fig. 6 C). These data show that mitochondrial ROS production during reoxygenation is dependent on expression of UQCRC2 but that, only in cNLRX1 cells, this also results in increased apoptosis.

A recent study identified the polyunsaturated fatty acid docosahexaenoic acid (DHA) as one of three fatty acid ligands for NLRX1 (Lu et al., 2015). Therefore we examined if DHA could reduce apoptosis after reoxygenation in an NLRX1-dependent fashion. Palmitate, a saturated fatty acid, was used as a control. In cEmpty cells treated with DHA, caspase-3 cleavage was not increased during reoxygenation compared with control-treated cells or cells treated with palmitate. In cNLRX1 cells, caspase-3 cleavage was not affected by both DHA and palmitate treatment during reoxygenation. These findings show that the unsaturated fatty acid DHA, but not the saturated fatty acid palmitate, reduces apoptosis in an NLRX1-dependent fashion during reoxygenation.

imaging of a kidney section obtained from an NLRX1 KO animal at day 1 after ischemia showing a phagosome-like structure containing mitochondria. Mitochondrial fragmentation (black arrows) and mitochondrial collapse (white arrows) are indicated; n, nucleus. (I) Transcription of glutathione peroxidase (GPX) 1 and 3, peroxiredoxin 1 (PRDX1), and superoxide dismutase 2 (SOD2) in kidney tissue from WT and KO animals (white and black bars, respectively, $n = 8$ per group) at the indicated time points during IRI. Bars, 500 nm, 1 µm, or 2 µm as indicated. Data are expressed as mean ± SEM and were analyzed using a Mann-Whitney *U* test (*, $P < 0.05$).

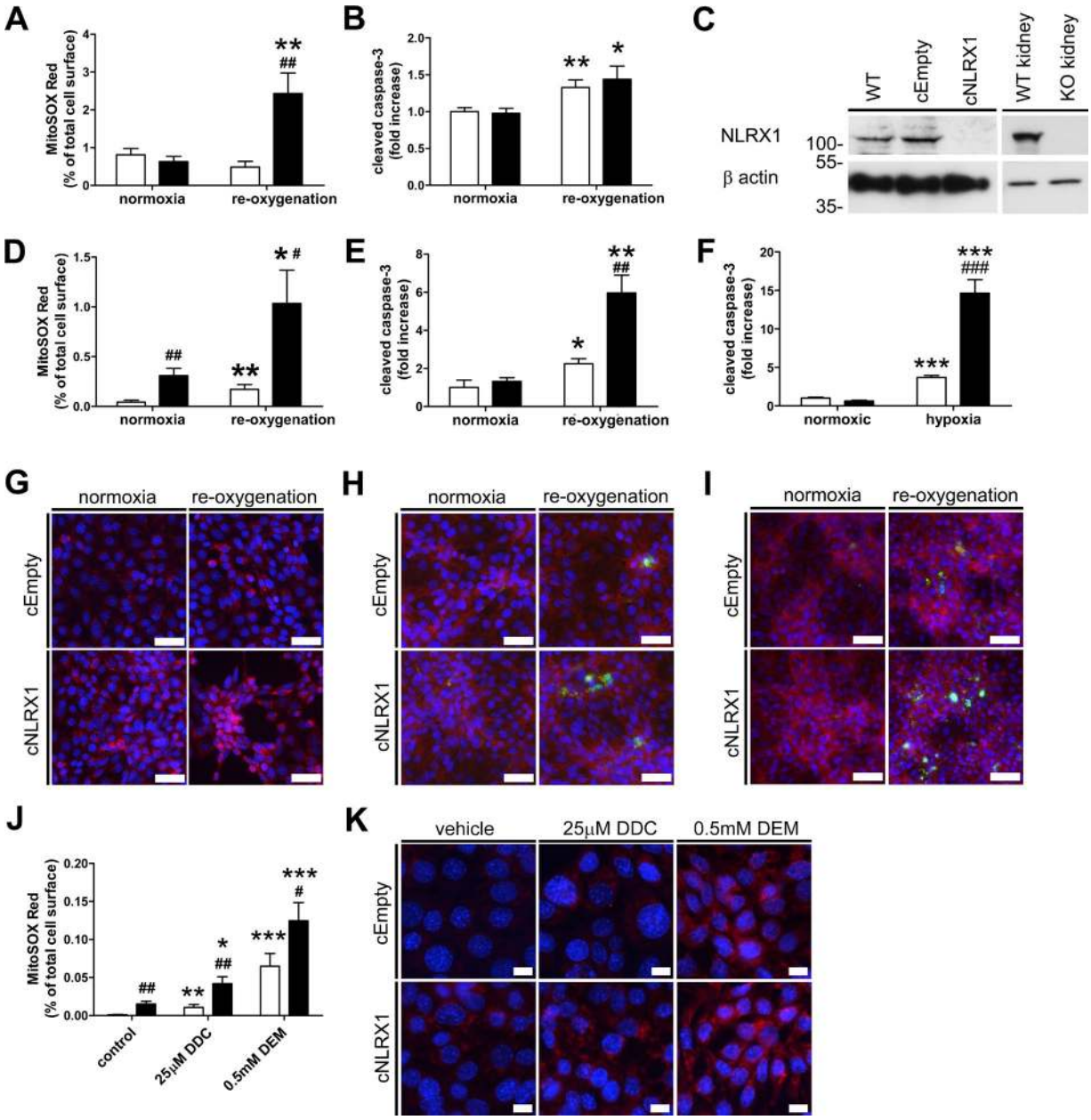

Figure 3. **Loss of NLRX1 increases ROS production and apoptosis after hypoxia.** Primary isolated TECs obtained from WT (white bars) or NLRX1 KO (black bars) mice were subjected to hypoxia and (A) labeled with MitoSOX Red for 45 min during reoxygenation and (B) stained for cleaved caspase-3 at 24 h of reoxygenation. (C) Western blot for NLRX1 on parental IM-PTEC, cEmpty, and cNLRX1 cells. WT and NLRX1 KO kidney was used as control. B actin was used as loading control. Protein molecular weight is indicated in kilodaltons. Digital image analysis of cEmpty (white bars) or cNLRX1 (black bars) cells subjected to hypoxia and (D) labeled with MitoSOX Red for 45 min during reoxygenation and (E) stained for cleaved caspase-3 at 24 h of reoxygenation. Representative images for (G) MitoSOX Red labeling (red) and a nuclear counterstain (blue) as analyzed in D and for (H) cleaved caspase-3 (green) with counterstains for F actin (red) and nuclei (blue) as analyzed in E. (F) Analysis of cleaved caspase-3 after 48 h in a hypoxic chamber and (I) representative images for cleaved caspase-3 (green) with counterstains for F actin (red) and nuclei (blue). (J) Digital image analysis of cells incubated for 3 h with the indicated compounds and labeled with MitoSOX Red. DDC, diethyldithiocarbamate; DEM, diethyl maleate. (K) Representative images with MitoSOX Red labeling (red) and a nuclear counterstain (blue) used for analysis presented in J. Data are expressed as mean ± SEM and were analyzed using an unpaired *t* test or ANOVA (nephrotoxicants; *, $P < 0.05$; **, $P < 0.01$; ***, $P < 0.001$ vs. respective normoxic control; #, $P < 0.05$; ##, $P < 0.01$; ###, $P < 0.001$ vs. cEmpty control). All conditions were determined in triplicate; representative data from three independent experiments are shown. Bars, 50 μm (G–I) and 10 μm (K).

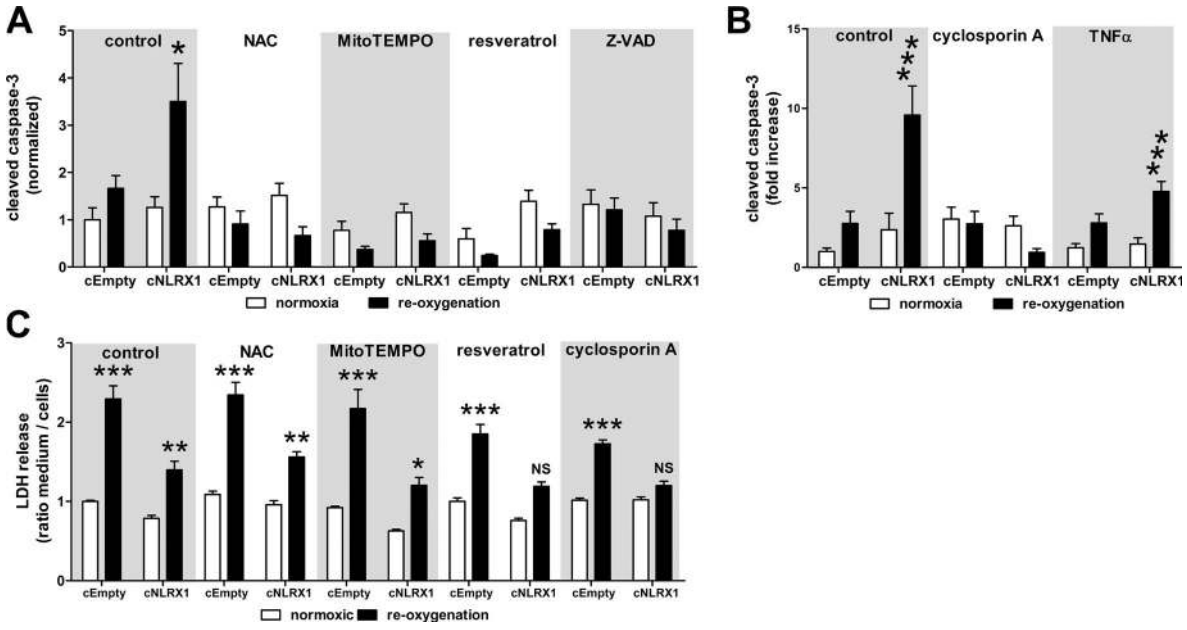

Figure 4. **Antioxidant treatment reduces apoptosis in cNRX1 cells.** (A) Cells were treated with the indicated antioxidant compounds for 24 h under normoxic conditions (white bars) or after hypoxia (black bars). Cleaved caspase-3 staining was analyzed by digital image analysis. NAC, N-acetyl cysteine. (B) Cells were treated with the indicated compounds for 24 h under normoxic conditions (white bars) or after hypoxia (black bars). Cleaved caspase-3 staining was analyzed by digital image analysis. (C) Cells were treated with the indicated antioxidant compounds for 24 h under normoxic conditions (white bars) or after hypoxia (black bars). LDH levels in conditioned medium and cell fraction were determined and expressed as the ratio of medium LDH over cellular LDH. All data are expressed as mean ± SEM and were analyzed using an unpaired *t* test (*, $P < 0.05$; **, $P < 0.01$; ***, $P < 0.001$ vs. respective normoxic control; N.S., not significant). All conditions were determined in triplicate; representative data from three independent experiments are shown.

Decreased NLRX1 expression during acute tubular necrosis and acute cellular rejection in patients

Decreased NLRX1 expression was associated with severity of lung injury in COPD patients (Kang et al., 2015). We therefore examined tubular NLRX1 expression by immunohistochemistry on biopsy material from patients diagnosed with acute tubular necrosis (ATN) or acute cellular rejection (ACR). ATN results most commonly from renal IRI (Devarajan, 2006), whereas ACR involves a T cell–specific allo-immune response that is triggered by prior ischemia and delayed graft function (Menke et al., 2014). As controls we used protocol biopsies taken at 6 mo after transplantation from normally functioning transplanted kidneys and pretransplantation kidney allografts.

In normal kidney tissue, tubules showed clear cytoplasmic NLRX1 labeling (Fig. 7 A). We observed strong NLRX1 labeling in smooth muscle cells lining renal blood vessels (Fig. 7 B). In contrast, NLRX1 expression was absent or low in biopsies diagnosed with ATN (Fig. 7 C) or ACR (Fig. 7 D), showing that NLRX1 is significantly decreased in tubular injury (Fig. 7 F). Interestingly, we did find that NLRX1 expression was present in inflammatory cells in ACR biopsies (Fig. 7 E).

DISCUSSION

The rapidly expanding field of immunometabolism investigates the interaction between metabolic switches and immunological activity of cells. Immune activation may drastically alter a cell's metabolic signature to support cell proliferation and increased functional activity, for example during T lymphocyte activation (Wang et al., 2011) and dendritic cell activation (Everts et al., 2014). In this study we provide a novel connection of NLRX1, a designated innate immune system receptor, with control of epithelial cellular metabolism during conditions of cytotoxic cell stress. Although first implicated in immune regulation, we find that NLRX1 function may be extended to control of mitochondrial activity and prevention of apoptosis in peripheral tissue injury. Our results show that NLRX1 expression regulates oxidative stress in renal IRI by controlling mitochondrial activity and oxygen consumption, consequently regulating TEC apoptosis. Loss of NLRX1 in animal and cell models significantly increased expression of markers for mitochondrial oxidative stress during IRI and was accompanied by severe mitochondrial morphological alterations. The central role of mitochondrial dysfunction leading to oxidant production and apoptosis was further demonstrated by the antiapoptotic effect of antioxidants and CsA-mediated inhibition of the mitochondrial transition pore in NLRX1 KO cells. This suggests that loss of NLRX1 is associated with increased tissue injury. Suppression of NLRX1 occurs in chronic obstructive pulmonary disease and was associated with increased disease severity (Kang et al., 2015). Similarly, we observed a transient reduction in NLRX1

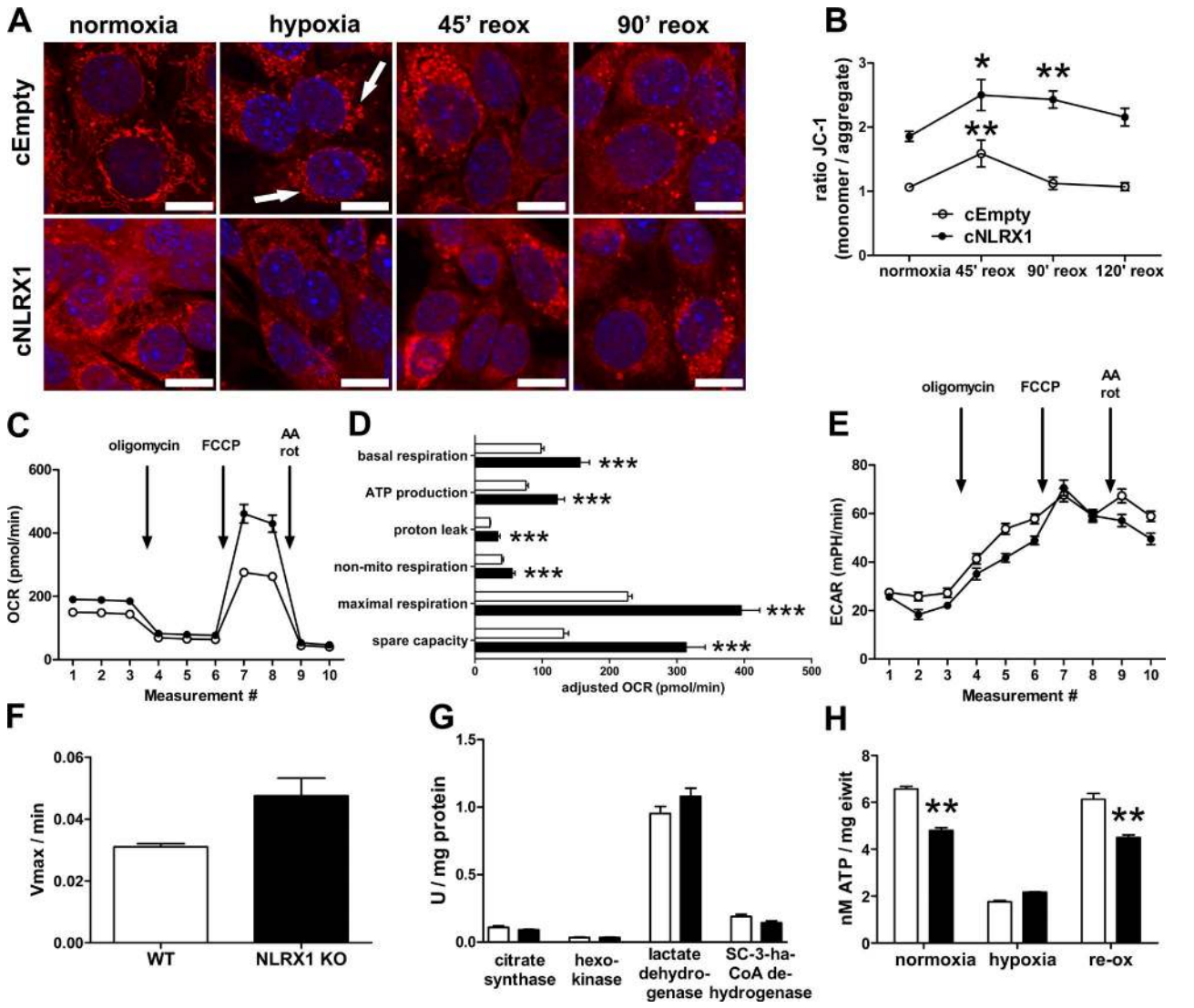

Figure 5. **Loss of NLRX1 disrupts mitochondrial morphology but increases mitochondrial activity.** (A) Confocal microscopic images of cEmpty (top) and cNLRX1 cells (bottom) labeled with MitoTracker Deep Red (red) at the indicated time points. Nuclei (blue) were counterstained; bars, 10 µm. White arrows indicate examples of mitochondrial fragmentation. Conditions were examined in triplicate; representative images are shown. reox, reoxygenation. (B) Analysis of mitochondrial membrane potential using JC-1 labeling under normoxic conditions or at indicated time points after hypoxia for cEmpty cells (open circles) and cNLRX1 cells (closed circles). All conditions were examined in sixfold. Representative data from three independent experiments are shown. (C) Seahorse Bioanalyzer OCR readout of a typical mitochondrial function assay using cEmpty (open circles) and cNLRX1 (closed circles) without adjustment for cell number. AA, antimycin A; rot, rotenone. Conditions were determined in sixfold; representative data from three independent experiments are shown. (D) OCR data from C adjusted for cell input for cEmpty cells (white bars) and cNLRX1 cells (black bars). (E) Seahorse Bioanalyzer extracellular acidification rate (ECAR) readout of a typical mitochondrial function assay using cEmpty cells (open circles) and cNLRX1 cells (closed circles) without adjustment for cell number. Conditions were determined in sixfold. Representative data from three independent experiments are shown. (F) Complex II/III activity determined in isolated kidney mitochondria from WT (white bars) and NLRX1 KO mice (black bars; $n = 3$ per group). (G) Enzyme activity of citrate synthase, hexokinase, LDH, and SCHAD determined in normoxic cEmpty and cNLRX1 cells. All conditions were examined in triplicate; representative data from three independent experiments are shown. (H) ATP levels in cEmpty cells (white bars) and cNLRX1 cells (black bars) were measured at the indicated time points and adjusted to total protein contents per sample. Conditions were examined in sixfold. Representative data from three independent experiments are shown. All data are expressed as mean ± SEM and were analyzed using an unpaired *t* test except enzyme activity by Mann-Whitney *U* test (*, $P < 0.05$; **, $P < 0.01$; ***, $P < 0.001$).

transcription during renal IRI in WT animals and in biopsies from patients diagnosed with ATN and ACR, suggesting that loss of NLRX1 may be involved in initiation of the injury response to renal ischemia and may result from a general reduction in transcription of genes that are not directly involved in cellular support or repair after injury. Finally, we found no clear difference in the degree of tubular necrosis between WT and NLRX1 KO mice (Fig. 1, B and L), suggesting that other

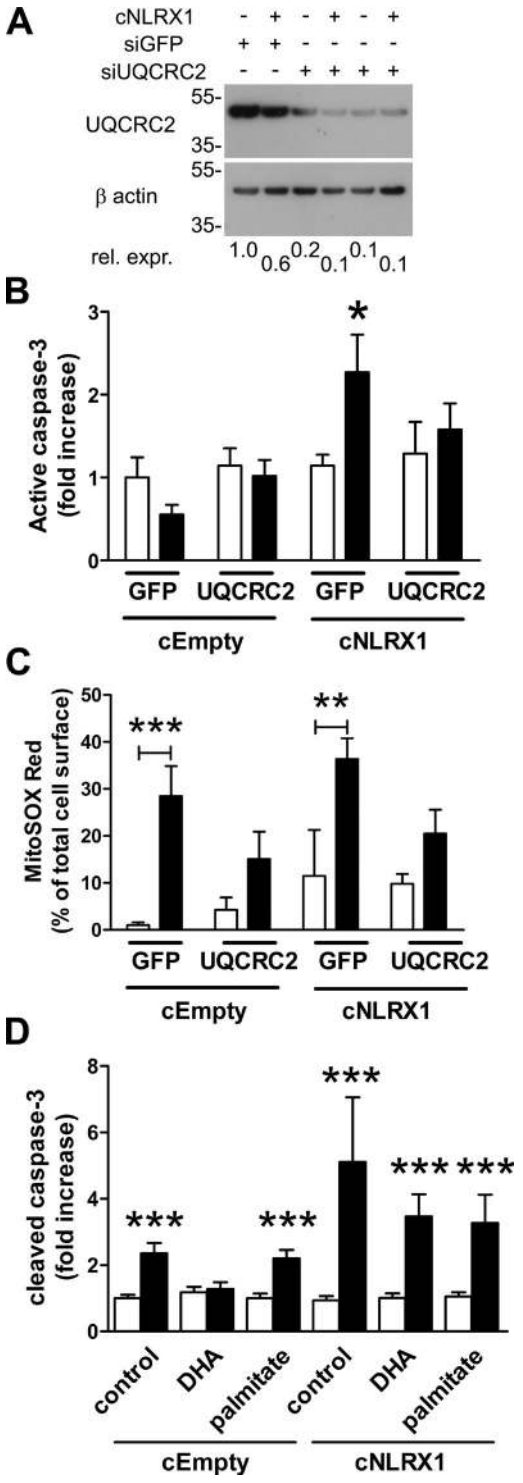

Figure 6. **Knockdown of UQCRC2 and exposure to polyunsaturated fatty acid prevents apoptosis in cNLRX1 cells.** (A) Western blot analysis of UQCRC2 expression in cEmpty and cNLRX1 cells treated with siGFP or siUQCRC2, as indicated. Relative expression (Rel. expr.) for UQCRC2 was determined by densitometric analysis for UQCRC2 and respective β actin bands. Protein molecular weight is indicated in kilodaltons. (B and C) Cells were treated with the indicated siRNA and subjected to hypoxia followed by reperfusion for 24 h. (B) Cleaved caspase-3 staining and (C) MitoSOX Red were analyzed by digital image analysis for normoxia (white bars) and reoxygenation (black bars) samples. (D) Cleaved caspase-3 staining was analyzed by digital image analysis for normoxia (white bars) and reoxygenation (black bars) during 24 h of exposure to the indicated fatty acids. Data are expressed as mean ± SEM and were analyzed using an unpaired *t* test (*, $P < 0.05$; **, $P < 0.01$; ***, $P < 0.001$ vs. normoxic control). All conditions were determined in triplicate; representative data from three independent experiments are shown.

mechanisms, besides loss of NLRX1 expression, are more involved in necrotic cell death in renal IRI. We observed a slight decrease in LDH release in cNLRX1 cells during reoxygenation compared with cEmpty cells. An explanation could be that, in contrast to our in vivo model in which necrosis may be induced by granulocyte activation (Jansen et al., 2017), in vitro LDH release can only be the result of reoxygenation.

Recently, NLRX1 was shown to be a regulator of apoptosis in tumor and transformed cells (Soares et al., 2014; Singh et al., 2015). Loss of NLRX1 in tumor cells or SV40-transformed cells, but not in nontransformed cells, increased susceptibility to cell death induced by TNF combined with cycloheximide (Soares et al., 2014). We found that TNF exposure during reoxygenation did not increase apoptosis in our NLRX1 KO cells compared with normoxic controls. We used a conditionally immortalized cell line, which was used for cell assays after 1-wk culture under restrictive conditions, resulting in loss of SV40 expression (Stokman et al., 2011). Therefore our findings are in line with studies that show that NLRX1 decreases susceptibility to extrinsic apoptosis in SV40-transformed cells only. In contrast, the study by Singh et al. (2015) shows that introduction of NLRX1 in HEK293 cells increases TNF-induced cell death. In addition they found that NLRX1 expression, rather than loss of NLRX1 expression, is responsible for increased oxidative stress upon TNF stimulation but suggested that this is dependent on caspase-8 activation and failed to show a direct correlation between oxidative stress and apoptosis.

NLRX1 was initially implicated in regulation of antiviral immunity by blocking association of TRAF6 to IκK (Allen et al., 2011; Xia et al., 2011). We found no clear effect of NLRX1 deletion on inflammatory cell accumulation in comparison with WT animals during IRI, with the exception of chemokine production (Fig. 1, E–H). Expression of CXCL1 and CCL2 by proximal TECs during IRI is dependent on functional TLR2 activation (Leemans et al., 2005), upstream of NF-κB activation. We therefore cannot completely rule out that NLRX1 is involved in negative regulation of NF-κB signaling during IRI. However, our data clearly point toward mitochondrial dysfunction and increased ROS production as the principal mechanism behind the increase in tubular epithelial apoptosis in mice and cells that lack NLRX1. In addition, by using BM chimeric animals, we established that loss of renal NLRX1, but not BM NLRX1, results in increased tubular epithelial apoptosis.

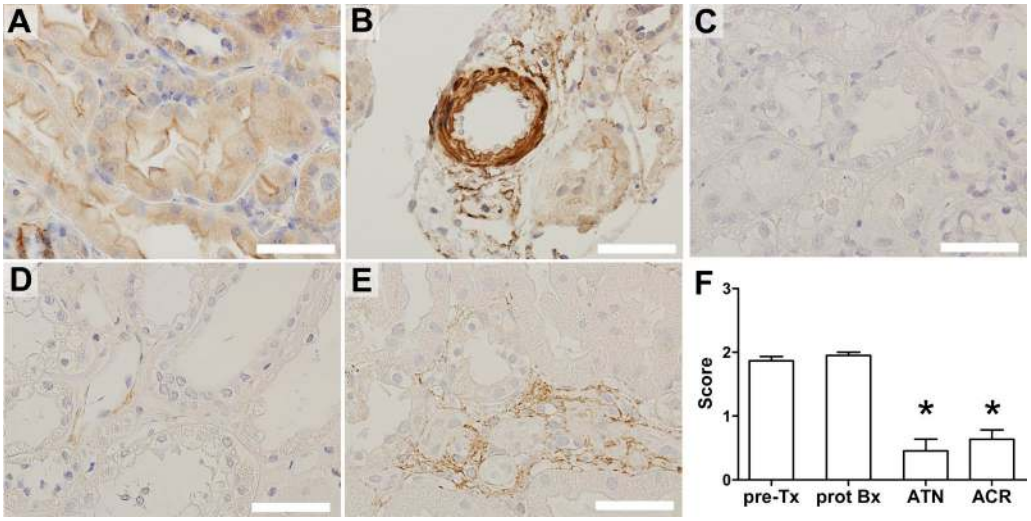

Figure 7. **Decreased tubular NLRX1 expression in ATN and ACR biopsies.** (A) Representative example of NLRX1 immunostaining performed on a protocol biopsy at 6 mo after renal transplantation. Expression of NLRX1 by (B) renal vascular smooth muscle cells. Absent or low NLRX1 labeling in biopsies diagnosed with (C) ATN and (D) ACR. (E) NLRX1 expression by inflammatory cells but not tubular epithelium in ACR. (F) Semiquantitative scoring of tubular staining intensity for NLRX1. Data are expressed as mean ± SEM and were analyzed using a Mann-Whitney *U* test (*, $P < 0.05$ vs. both controls). Pre-Tx, pretransplantation kidney ($n = 3$); prot Bx, protocol biopsy at 6 mo after transplantation ($n = 4$); ATN ($n = 11$) and ACR ($n = 10$). Bars, 50 µm.

A recessive inactivating mutation in the *UQCRC2* gene found in related individuals resulted in neonatal onset of hypoglycemia, lactic acidosis, ketosis, and hyperammonemia and was the basis for complex III functional deficiency (Miyake et al., 2013). Its exact role in regulation of OXPHOS remains unknown, but UQCRC2 has been classified as a pseudomitoprotease, comprising a group of catalytically deficient mitochondrial proteases with a regulatory function (Quirós et al., 2015). We found that loss of NLRX1 increased OXPHOS in cells and tissue, suggesting that NLRX1-mediated regulation of UQCRC2 is responsible for control of complex III activity. We found that increased apoptosis in NLRX1 KO cells after hypoxia was dependent on accumulation of ROS. In line with this, siRNA-mediated knockdown of UQCRC2 suppressed apoptosis of NLRX1-deficient cells, providing evidence for a direct or indirect interaction between NLRX1 and UQCRC2 resulting in decreased complex III activity. Knockdown of UQCRC2 may affect complex III formation and activity and could therefore negatively influence ROS production merely by disruption of the electron transport chain. However, pharmacological inhibition of complex III by antimycin A increased apoptosis 10-fold in cEmpty and cNLRX1 cells compared with control-treated cells (unpublished data). Thus UQCRC2 deficiency may alter complex III formation with moderate effects on complex activity (Miyake et al., 2013) without complete electron transport chain disruption. In addition, we found that although OCR measurement hinted at increased ATP production in cNLRX1, ATP levels are significantly decreased in cNLRX1 cells compared with controls, suggesting increased ATP consumption by cNLRX1 cells or inefficient ATP synthesis. Depletion of ATP from proximal TECs during IRI is one of the principal mechanisms triggering mitochondrial ROS formation (Devarajan, 2006). Therefore decreased ATP levels in cNLRX1 cells may additionally contribute to increased ROS formation and apoptosis. Our results are in line with those of Singh et al. (2015), who showed that knockdown of NLRX1 is associated with increased complex III activity but does not increase ATP levels compared with control cells.

Surface plasmon resonance spectroscopy revealed that the polyunsaturated fatty acids DHA, punicic acid, and eleostearic acid bind the C-terminal end of the leucine-rich repeat domain of NLRX1 and modulate intestinal injury in an NLRX1-dependent way (Lu et al., 2015). These findings indicate that NLRX1 activity can be modulated by fatty acid levels. We found that the polyunsaturated fatty acid DHA, but not the saturated fatty acid palmitate, prevented apoptosis during reoxygenation dependent on NLRX1 (Fig. 6 D), confirming that polyunsaturated fatty acids modulate NLRX1 function. Several studies demonstrate the anti-inflammatory properties of DHA and its metabolites in models for kidney injury (Duffield et al., 2006; Li et al., 2017). Although we found that DHA decreases apoptosis in an NLRX1-dependent fashion using a cell model for AKI, we acknowledge that DHA is not a selective ligand for NLRX1. For example, DHA metabolites inhibited NLRP3 inflammasome activation in a model for glomerular injury (Li et al., 2017). In addition, DHA may act on different cell types, as DHA-derived resolvins primarily decreased activation of inflammatory cells in AKI (Duffield et al., 2006). The lack of pharmacological activators or inhibitors is therefore a limitation of the present study. Concerning the other NLRX1 ligands described by Lu et al. (2015), we were

unable to find a reliable commercial source for punicic acid without contaminating impurities, and we did not examine eleostearic acid, because the original study did not fully investigate how this fatty acid acts on intestinal injury compared with DHA and punicic acid.

We found that in epithelial cells, NLRX1 may act as an inhibitor of mitochondrial activity and blocks excessive oxidative stress in a model for AKI. In contrast to other pattern recognition receptors that worsen outcomes by triggering immune response activation, NLRX1 is to our knowledge the first pattern recognition receptor that has a protective role in renal tissue injury. Our study challenges current ideas on NLRX1 function and proposes a direct link between an innate immune receptor and control of mitochondrial function.

MATERIALS AND METHODS

Reagents and antibodies

Rat-anti–mouse-Gr-1 (cat 553126; BD), -CD45.1 (cat 553772; BD) and -CD45.2 (cat 552950; BD), rabbit-anti–mouse-NLRX1 (cat 17215-1-AP; ProteinTech), rat-anti–mouse-F4/80 (cat MCA497; AbD Serotec), mouse-anti–mouse-β actin (cat A5316; Sigma-Aldrich), rabbit-anti–human-NLRX1 (cat HPA038630; Sigma-Aldrich), and rabbit-anti–mouse-UQCRC2 (cat SAB1411387; Sigma-Aldrich), rabbit-anti–cleaved caspase-3 (cat 9661; Cell Signaling Technology), rabbit-anti–human-NLRX1 (cat ab107611; Abcam) and 4-hydroxynonenal (cat ab46545; Abcam), and nitrosylated tyrosine (cat AB5411; EMD Millipore) were purchased. Secondary Alexa Fluor 488– and Alexa Fluor 594–labeled antibodies were purchased from Thermo Fisher Scientific. Antimycin A, CsA, *N*-acetyl-cysteine, MitoTEMPO, resveratrol, Hoechst 33342, NADH, sodium pyruvate, diethyldithiocarbamate, diethyl maleate, palmitate, and cis-4,7,10,13,16,19-DHA were purchased from Sigma-Aldrich. Recombinant mouse TNF-α was purchased from ProSpec. Paraffin oil (paraffin liquidum, 110–230 mPa·s) was from Spruyt-Hillen.

Mice and animal experimental procedures

Homozygous NLRX1 KO mice were generated as described previously (Soares et al., 2013) from B6.C-Tg(CMV-cre)1Cgn/J mice and congenic NLRX1 floxed B6 mice and bred at our institute. Age-matched (8–10-wk-old) male WT C57BL6/J were obtained from Charles River. All animals received food and water ad libitum. Mice were anesthetized using Midazolam (Actavis) and Hypnorm (Vetapharma) and maintained on heat pads for the whole duration of the procedure. To induce renal IRI, an abdominal midline incision was made and renal pedicles were clamped using nontraumatic vascular clips. For bilateral IRI, pedicles were clamped for 20 min (n = 8 for WT mice and NLRX1 KO mice) or 25 min for BM chimeric mice (n = 7 per group; see below). Sham-operated animals (n = 2 per group) received identical treatment without clamping of the renal pedicles. For unilateral IRI, the left pedicle was clamped for 30 min (n = 8 per group), whereas the contralateral kidney served as an internal control. Restoration of renal perfusion was confirmed after release of clamps by visual inspection. The abdomen was irrigated with a sterile saline solution, after which the incision was closed using nonabsorbable sutures (6.0; Tyco Healthcare). All mice received a subcutaneous injection of 0.1 mg/kg Temgesic (Schering-Plough) postoperatively. Animals were sacrificed at day 1 or 5 after ischemia by heart puncture for blood collection under isoflurane anesthesia followed by cervical dislocation. Blood samples were transferred to lithium-heparin gel tubes. Kidneys were collected and fixed in formalin (for immunohistochemistry), in Karnovsky solution (for electron microscopy) or snap-frozen in liquid nitrogen for further processing.

For isolation of primary TECs, kidneys were removed and maintained on ice in HBSS supplemented with 50 U penicillin and 50 µg/ml streptomycin. The renal capsule was removed and tissue minced using scalpels. A single-cell suspension was made using collagenase digestion in DMEM/F12 medium for 30 min at 37°C, cell straining over a 70- and 40-µm filter mesh and cultured in HK-2 medium (see below) for up to 1 wk under normal culture conditions.

All experimental procedures were approved by the Animal Care and Use Committee of the Academic Medical Center. All animals received food and water ad libitum.

Generation of BM chimeric mice

Total BM was collected from donor mice by flushing femurs and tibiae with sterile PBS supplemented with 10% FCS (Invitrogen) and penicillin (50 U/ml)/streptomycin (50 µg/ml; Invitrogen). Recipient mice were lethally irradiated with two doses of 4.5 Gy, divided by 3 h minimally, using a ^{137}Cs irradiator (CIS Bio International). After the last irradiation dose, mice received an intravenous injection of total volume of 300 µl per mouse containing 5×10^6 donor BM cells and 2×10^5 spleen cells of the recipient strain to induce acute radioprotection. Three groups were created: BM from NLRX1 KO mice into WT recipients (KO → WT), BM from WT mice into NLRX1 KO recipients (WT → KO), and BM from WT mice into WT recipients (WT → WT).

For 6 wk after transplantation, mice received sterile acidified tap water (12 mM HCl) that contained 0.16% neomycin sulfate (Sigma-Aldrich). Functional BM engraftment was determined by expression analysis of CD45.1 (WT C57BL6/J animals) and CD45.2 (NLRX1 KO animals) by peripheral leukocytes using a FACSCalibur (BD Biosciences) flow cytometer. Chimeras with donor BM engraftment of >75% or higher were used for further experiments. Note that this approach was not used for WT → WT control BM transplantation animals. No gross hematological abnormalities were detected in all animals after transplantation.

Histopathological analysis and measurement of renal function and LDH

For histopathology scoring, sections were stained with periodic acid-Schiff reagents after diastase digestion. Tubular ne-

crosis was determined by a pathologist in a blinded fashion by quantifying the percentage of affected tubules per 10 high power fields in the corticomedullary region graded on a scale from 0–5: 0 = 0%; 1 = <10%; 2 = 10%–25%; 3 = 25%–50%; 4 = 50%–75%; and 5 = >75%. Plasma LDH was measured at the Department of Clinical Chemistry of our institution in a routine fashion using CREA plus (Roche). NLRX1 expression was determined on patient renal biopsies that were taken according to protocol at 6 mo after kidney transplantation (n = 4), pretransplantation grafts that were not approved for transplantation (n = 3), and biopsies of patients diagnosed with ATN (n = 11) or ACR after kidney transplantation (n = 10). All biopsy material was fixed in formalin before paraffin embedding. NLRX1 immunohistochemical staining was scored semiquantitatively using a scale from 0–3: 0 = no staining; 1 = low staining intensity; 2 = intermediate staining intensity; 3 = high staining intensity. All renal biopsies were taken for diagnostic purposes only. This research project used only leftover biological material, anonymous and delinked from patient records, and as such was not subject to any requirement for ethical review or approval.

Immunohistochemistry and ELISA

For paraffin embedding, tissue samples were fixed for 24 h in formalin and processed in a Tissue-Tek VIP (Sakura). Tissue sections (4 µm thick) were dewaxed, and sections were treated with 0.3% hydrogen peroxide in methanol for 15 min. For cleaved caspase-3, 4-hydroxynonenal and nitrosylated tyrosine and NLRX1 stainings, sections were boiled for 10 min in a citrate buffer, pH 6.0, and for the Gr-1 and F4/80 staining incubated in a pepsin buffer (0.01 U/ml) at 37°C for 15 min. Sections were blocked with Ultra V block (Thermo Fisher Scientific) for 30 min and incubated with primary antibodies overnight at 4°C. Sections were incubated with HRP-conjugated secondary antibodies for 30 min. Antibodies and blocking solution were diluted in PBS. Sections were stained with 3,3-diaminobenzidine, and alternatively, nuclei were counterstained with hematoxylin or methylene green. Images were obtained using an Olympus BX51 microscope (lenses: UPlanFl 20×/0.50 and UPlanAPO 40×/0.85) fitted with a DP70 camera and the provided acquisition software (Olympus).

Frozen tissue was lysed in Greenberger lysis buffer (300 mM NaCl, 30 mM Tris, 2 mM $MgGl_2$, 2 mM $CaCl_2$, and 1% Triton X-100, pH 7.4, supplemented with Protease Inhibitor Cocktail II; Sigma-Aldrich). Duoset ELISAs for CXCL1 (KC) and CCL2 (MCP1) were from R&D Systems and performed according to the supplied protocol. Data were adjusted for total protein concentration as determined by bicinchoninic acid protein assay (Thermo Fisher Scientific).

Mitochondrial isolation and determination of complex II/III activity

Kidney mitochondria were isolated as described by Frezza et al. (2007). In short, kidneys were taken from WT and NLRX1 KO mice and maintained on ice in a buffer containing 0.2 M sucrose, 0.01 M Tris, and 1 mM EGTA. Tissue was minced and homogenized using a glass-Teflon potter. Mitochondria were collected after centrifugation at 7,000 *g*, as described by Frezza et al. (2007). Complex II/III activity was determined using the MitoTox OXPHOS complex II+III activity kit (Abcam) according to the provided protocol. Cytochrome *c* reduction was measured at 550 nm using a ClarioSTAR plate reader. Data were expressed as Vmax, defined as delta mOD per minute.

Cells and cell culture

All cells were cultured in HK-2 medium (DMEM/F12 medium [Invitrogen] with 10% FBS [Invitrogen], 5 µg/ml insulin and transferrin, 5 ng/ml sodium selenite [Thermo Fisher Scientific], 20 ng/ml triiodo-thyrionine [Sigma-Aldrich], 50 ng/ml hydrocortisone [Sigma-Aldrich], and 5 ng/ml prostaglandin E1 [Sigma-Aldrich] with L-glutamine and antibiotics [both from Invitrogen]). Conditionally IM-PTECs (Stokman et al., 2010) were cultured at 33°C in the presence of 10 ng/ml IFN-γ (ProSpec) and maintained at 37°C without IFN-γ for an additional week before start of the assay, resulting in loss of SV40 expression (Stokman et al., 2011). Primary TECs were isolated and cultured as described above.

For generation of NLRX1 KO cells, we used CRI SPR/Cas9-mediated KO. The following guide strands were cloned in the LentiCRISPR vector v2 (Addgene): 5′-CAC CGCAGGGATAGATTGGACGTGT-3′ and 5′-AAACAC ACGTCCAATCTATCCCTGC-3′. The resulting plasmid was transfected into HEK293T cells together with pVSVg and psPAX2 (both from Addgene) using Genius transfection reagent (Westburg). Supernatant of transfected cells containing viral particles was supplemented with 8 µg/ml polybrene (Sigma-Aldrich) and added to IM-PTECs cultured under permissive conditions for 24 h. After puromycine selection, cells were cultured as described above, and protein KO was confirmed by Western blotting.

For siRNA-mediated protein knockdown, cells were transfected with 50 nM siRNA specific for GFP (GFP Duplex I) or UQCRC2 (SMARTpool Accell; GE Healthcare) using INTERFERrin transfection reagents (Polyplus-transfection) for 6 h. Cells were maintained in HK-2 medium with 5% FCS for 2 d until the start of the assay.

RNA isolation and real-time PCR

Frozen tissue was lysed in TriReagent, and RNA was precipitated by isopropanol after chloroform phase separation. cDNA was synthesized using M-MLV reverse transcription (Thermo Fisher Scientific). Transcription was analyzed using real-time quantitative PCR on a LightCycler480 (Roche). Primers (Table 1) were synthesized by Eurogentec.

Cell assays

In vitro hypoxia-reoxygenation injury was induced as described previously (Stokman et al., 2014) by paraffin oil submersion for 60 min. Reoxygenation was induced by re-

placement of the oil layer by culture medium for 45 min (acute) or 24 h (long term). To examine mitochondrial superoxide production, cells were labeled with 1 µM MitoSOX Red (Thermo Fisher Scientific) for 45 min. For incubation in nitrogen gas, cells maintained in normal culture medium were placed in a Modular Incubator Chamber (Billups Rothenberg), which was flushed for 10 min with nitrogen (5 liters/min). After sealing, the chamber was placed in a standard cell incubator for 48 h. Normoxic controls were maintained under normal culture conditions.

To examine nephrotoxicant-induced oxidative stress, cells were incubated for 3 h with sodium diethyldithiocarbamate trihydrate or diethyl maleate (both from Sigma-Aldrich) and with MitoSOX Red for the last 45 min.

DHA and palmitate were conjugated to 2% (wt/vol) fatty acid–free, low-endotoxin BSA (Sigma-Aldrich) in DMEM/F12 medium at 37°C for 60 min and used for cell stimulation at a 50 µM concentration in HK-2 medium containing 2.5% FCS.

To determine LDH, 50 µl of cell-conditioned medium was added to 50 µl fresh medium containing 0.4% Triton X-100, mixed and added to 200 µl substrate buffer (100 mM sodium phosphate, 12.5 mM β-nicotinamide adenine dinucleotide, and 1.13 mM sodium pyruvate, pH 7.5). Absorbance was measured directly and after 10 min at 340 nm using a CLARIOstar plate reader (BMG LABTECH).

For mitochondrial membrane polarity measurement, cells were plated in black 96-well µClear plates (Greiner) and subjected to hypoxia-reoxygenation as described above. Mitochondrial polarity was determined using the MITO-ID Membrane potential cytotoxicity kit (Enzo Life Sciences). Dual fluorescence was measured using a CLARIOstar plate reader. Data are expressed as the ratio between JC-1 monomer (514 nm Ex/529 nm Em) and aggregate (514 nm Ex/590 nm Em).

To determine cellular oxygen consumption, cells were plated in the provided 96-well assay plates 1 d before the start of the assay. Mitochondrial function was determined using the XF Cell Mito Stress Test as described in the provided protocol, and OCR and extracellular acidification rate were measured on a XFe96 Extracellular Flux Analyzer (Seahorse Bioscience). Values were adjusted for total cell input per well using a crystal violet cell staining. In short, cells were stained with 0.4% crystal violet in methanol, washed with deionized water, and eluted with methanol. Absorbance of crystal violet was measured at 570 nm.

Immunofluorescence and microscopy

Cells were cultured on 12-mm glass coverslips. For mitochondrial labeling, cells were incubated with MitoTracker DeepRed (Thermo Fisher Scientific). Cells were fixed in 4% phosphate-buffered formaldehyde. Kidney tissue cryosections (10 µm) were fixed in acetone. Antibody labeling was done in PBS with 0.5% BSA and 0.1% Triton X-100. Cells were counterstained with FITC or Texas-Red-labeled phalloidin (Thermo Fisher Scientific) and/or Hoechst 33342 (Sigma-Aldrich). Coverslips were mounted on glass slides using Aqua-Poly/Mount (Polysciences). Epifluorescence microscopy was performed on a Leica DM5000B (lenses: 20×/0.70 and 63×/1.40–0.60), and confocal laser scanning microscopy (lens: 63×/1.40) was performed on a Leica TCS SP8 X, both using the LAS X acquisition software package (Leica).

For transmission electron microscopy, tissue was collected in Karnovsky fixative and postfixed in 1% osmium tetroxide. Tissue samples were block-stained with 1% uranyl acetate, dehydrated in dimethoxypropane, and embedded in epoxyresin LX-112. Light microscopy sections were stained with toluidine blue. Electron microscopy sections were stained with tannic acid, uranyl acetate, and lead citrate and examined using a Philips CM10 transmission electron microscope (FEI). Images were acquired using a digital transmission Morada 10–12 electron microscopy camera (Soft Imaging System) using the Research Assistant software package (RVC). We scored morphological disruption of mitochondria on a semiquantitative scale (0–3): 0 = no injury normal morphology, compact electron dense structure; 1 = mild injury: decrease in number of cristae, light swelling, loss of electron dense appearance, 2 = severe injury: (near) complete loss of cristae, severe swelling of mitochondria; 3 = complete disruption: rupture of the outer membrane, collapse of the mitochondrial structure. All mitochondria per five individual fields (18,500× magnification) per sample were scored, and the mean score per field was plotted.

Enzyme activity

Cells were collected and lysed in 0.5% (wt/vol) Triton X-100. Activity of citrate synthase, hexokinase, and LDH was deter-

Table 1. **Primer sequences used for quantitative PCR analysis**

Gene	Full name	Forward primer (5′–3′)	Reverse primer (5′–3′)
TBP	TATA box binding protein	GGAGAATCATGGACCAGAAC	GATGGGAATTCCAGGAGTCA
GAPDH	Glyceraldehyde 3-phosphate dehydrogenase	TGTCCGTCGTGGATCTGAC	CCTGCTTCACCACCTTCTTG
PPIA	Peptidylprolyl isomerase A	TGCCAGGGTGGTGACTTTAC	GATGCCAGGACCTGTATGCT
GPX1	Glutathione peroxidase 1	TTCGGACACCAGGAGAATGG	TAAAGAGCGGGTGAGCCTTC
GPX3	Glutathione peroxidase 3	CTCGGAGATACTCCCCAGTCT	TGGGAGGGCAGGAGTTCTTC
PRDX1	Peroxiredoxin 1	GGTATCCTGCTCCCAACTTCA	ATCTCCGTGGGACACACAAA
SOD2	Superoxide dismutase 2	ACAACTCAGGTCGCTCTTCAG	TCCAGCAACTCTCCTTTGGG
NLRX1	NOD-like receptor X1	TGCCATTTGCCCAGGACCTCTT	GCTCCACTGGATCAAGAAGGAGATATGC

mined as described previously (Zuurbier et al., 2005). Activity of short-chain-3-hydroxyacyl-CoA dehydrogenase was determined spectrophotometrically using MES, KH_2PO_4, DTT, NADH, and acetoacetyl-CoA, pH 6.2.

Western blotting

Cells and tissue were lysed in a buffer containing 10% glycerol, 1% Nonidet P40, 50 mM Tris-HCl, pH 7.4, 200 mM NaCl, 2.5 mM $MgCl_2$ and protease inhibitor cocktail II (Sigma-Aldrich). A 5× Laemmli sample buffer containing β-mercaptoethanol solution was added to the samples before boiling for 5 min, followed by protein separation and blotting on Immobilon-P (EMD Millipore). Immunoblots were blocked in Tris-buffered saline with 5% (wt/vol) ELK nonfat milk powder (FrieslandCampina) and incubated overnight with primary antibodies. For detection, immunoblots were incubated with peroxidase-conjugated secondary antibodies (Dako), and the presence of proteins was visualized using ECL (GE Healthcare) and exposure to Super Rx film (Fujifilm).

Statistics

Data are expressed as mean ± SEM. Data were tested using D'Agostino's K^2 normality test and analyzed using an unpaired Student's *t* test or Mann-Whitney *U* test for normal or non-Gaussian data distribution, respectively, or ANOVA combined with Bonferroni's post hoc test, as indicated in the figure legends. Necrosis, mitochondrial damage, and NLRX1 staining scores were analyzed using the Mann-Whitney *U* test. A p-value ≤ 0.05 was considered to indicate statistical significance. All statistical analyses were performed using GraphPad Prism 5 (GraphPad Software).

ACKNOWLEDGMENTS

G. Stokman is supported by a grant from the Dutch Kidney Foundation (13A3D301). P.J. Bakker, L. Kors, and E. Rampanelli are supported by a VIDI grant from the Netherlands Organization for Scientific Research (91712386 to J.C. Leemans).

The authors declare no competing financial interests.

Author contributions: G. Stokman designed and performed cell experiments, analyzed data, and wrote the paper. P.J. Bakker designed and performed animal experiments and analyzed data. L. Kors and E. Rampanelli performed cell experiments. N. Claessen and L. Butter provided technical support. M.A. van den Bergh Weerman and P.W.B. Larsen performed electron microscopy. C.J. Zuurbier, H. van Andel and M.C. Dessing provided analytical and experimental tools. G.J.D. Teske performed animal experiments. S.E. Girardin provided the mouse strains. S. Florquin provided biopsy material and histological analysis. J.C. Leemans designed experiments, analyzed data, supervised the project, and cowrote the paper.

Submitted: 5 July 2016
Revised: 22 March 2017
Accepted: 25 April 2017

REFERENCES

Allen, I.C. 2014. Non-inflammasome forming NLRs in inflammation and tumorigenesis. *Front. Immunol.* 5:169. http://dx.doi.org/10.3389/fimmu.2014.00169

Allen, I.C., C.B. Moore, M. Schneider, Y. Lei, B.K. Davis, M.A. Scull, D. Gris, K.E. Roney, A.G. Zimmermann, J.B. Bowzard, et al. 2011. NLRX1 protein attenuates inflammatory responses to infection by interfering with the RIG-I-MAVS and TRAF6-NF-κB signaling pathways. *Immunity.* 34:854–865. http://dx.doi.org/10.1016/j.immuni.2011.03.026

Arnoult, D., F. Soares, I. Tattoli, C. Castanier, D.J. Philpott, and S.E. Girardin. 2009. An N-terminal addressing sequence targets NLRX1 to the mitochondrial matrix. *J. Cell Sci.* 122:3161–3168. http://dx.doi.org/10.1242/jcs.051193

Bonventre, J.V., and L. Yang. 2011. Cellular pathophysiology of ischemic acute kidney injury. *J. Clin. Invest.* 121:4210–4221. http://dx.doi.org/10.1172/JCI45161

Devarajan, P. 2006. Update on mechanisms of ischemic acute kidney injury. *J. Am. Soc. Nephrol.* 17:1503–1520. http://dx.doi.org/10.1681/ASN.2006010017

Duffield, J.S., S. Hong, V.S. Vaidya, Y. Lu, G. Fredman, C.N. Serhan, and J.V. Bonventre. 2006. Resolvin D series and protectin D1 mitigate acute kidney injury. *J. Immunol.* 177:5902–5911. http://dx.doi.org/10.4049/jimmunol.177.9.5902

Everts, B., E. Amiel, S.C. Huang, A.M. Smith, C.H. Chang, W.Y. Lam, V. Redmann, T.C. Freitas, J. Blagih, G.J. van der Windt, et al. 2014. TLR-driven early glycolytic reprogramming via the kinases TBK1-IKKε supports the anabolic demands of dendritic cell activation. *Nat. Immunol.* 15:323–332. http://dx.doi.org/10.1038/ni.2833

Frezza, C., S. Cipolat, and L. Scorrano. 2007. Organelle isolation: functional mitochondria from mouse liver, muscle and cultured fibroblasts. *Nat. Protoc.* 2:287–295. http://dx.doi.org/10.1038/nprot.2006.478

Imbeault, E., T.M. Mahvelati, R. Braun, P. Gris, and D. Gris. 2014. Nlrx1 regulates neuronal cell death. *Mol. Brain.* 7:90. http://dx.doi.org/10.1186/s13041-014-0090-x

Ishimoto, Y., and R. Inagi. 2016. Mitochondria: a therapeutic target in acute kidney injury. *Nephrol. Dial. Transplant.* 31:1062–1069. http://dx.doi.org/10.1093/ndt/gfv317

Iyer, S.S., W.P. Pulskens, J.J. Sadler, L.M. Butter, G.J. Teske, T.K. Ulland, S.C. Eisenbarth, S. Florquin, R.A. Flavell, J.C. Leemans, and F.S. Sutterwala. 2009. Necrotic cells trigger a sterile inflammatory response through the Nlrp3 inflammasome. *Proc. Natl. Acad. Sci. USA.* 106:20388–20393. http://dx.doi.org/10.1073/pnas.0908698106

Jansen, M.P., D. Emal, G.J. Teske, M.C. Dessing, S. Florquin, and J.J. Roelofs. 2017. Release of extracellular DNA influences renal ischemia reperfusion injury by platelet activation and formation of neutrophil extracellular traps. *Kidney Int.* 91:352–364. http://dx.doi.org/10.1016/j.kint.2016.08.006

Kang, M.J., C.M. Yoon, B.H. Kim, C.M. Lee, Y. Zhou, M. Sauler, R. Homer, A. Dhamija, D. Boffa, A.P. West, et al. 2015. Suppression of NLRX1 in chronic obstructive pulmonary disease. *J. Clin. Invest.* 125:2458–2462. http://dx.doi.org/10.1172/JCI71747

Knott, A.B., G. Perkins, R. Schwarzenbacher, and E. Bossy-Wetzel. 2008. Mitochondrial fragmentation in neurodegeneration. *Nat. Rev. Neurosci.* 9:505–518. http://dx.doi.org/10.1038/nrn2417

Kopp, E.B., and R. Medzhitov. 1999. The Toll-receptor family and control of innate immunity. *Curr. Opin. Immunol.* 11:13–18. http://dx.doi.org/10.1016/S0952-7915(99)80003-X

Leemans, J.C., G. Stokman, N. Claessen, K.M. Rouschop, G.J. Teske, C.J. Kirschning, S. Akira, T. van der Poll, J.J. Weening, and S. Florquin. 2005. Renal-associated TLR2 mediates ischemia/reperfusion injury in the kidney. *J. Clin. Invest.* 115:2894–2903. http://dx.doi.org/10.1172/JCI22832

Leemans, J.C., L.M. Butter, W.P. Pulskens, G.J. Teske, N. Claessen, T. van der Poll, and S. Florquin. 2009. The role of Toll-like receptor 2 in inflammation and fibrosis during progressive renal injury. *PLoS One.* 4:e5704. http://dx.doi.org/10.1371/journal.pone.0005704

Leemans, J.C., L. Kors, H.J. Anders, and S. Florquin. 2014. Pattern recognition receptors and the inflammasome in kidney disease. *Nat. Rev. Nephrol.* 10:398–414. http://dx.doi.org/10.1038/nrneph.2014.91

Li, G., Z. Chen, O.M. Bhat, Q. Zhang, J.M. Abais-Battad, S.M. Conley, J.K. Ritter, and P.L. Li. 2017. NLRP3 inflammasome as a novel target for docosahexaenoic acid metabolites to abrogate glomerular injury. *J. Lipid Res.* 58:1080–1090. http://dx.doi.org/10.1194/jlr.M072587

Lu, P., R. Hontecillas, V. Abedi, S. Kale, A. Leber, C. Heltzel, M. Langowski, V. Godfrey, C. Philipson, N. Tubau-Juni, et al. 2015. Modeling-enabled characterization of novel NLRX1 ligands. *PLoS One.* 10:e0145420. http://dx.doi.org/10.1371/journal.pone.0145420

Martinon, F., K. Burns, and J. Tschopp. 2002. The inflammasome: a molecular platform triggering activation of inflammatory caspases and processing of proIL-beta. *Mol. Cell.* 10:417–426. http://dx.doi.org/10.1016/S1097-2765(02)00599-3

Menke, J., D. Sollinger, B. Schamberger, U. Heemann, and J. Lutz. 2014. The effect of ischemia/reperfusion on the kidney graft. *Curr. Opin. Organ Transplant.* 19:395–400. http://dx.doi.org/10.1097/MOT.0000000000000090

Miyake, N., S. Yano, C. Sakai, H. Hatakeyama, Y. Matsushima, M. Shiina, Y. Watanabe, J. Bartley, J.E. Abdenur, R.Y. Wang, et al. 2013. Mitochondrial complex III deficiency caused by a homozygous UQCRC2 mutation presenting with neonatal-onset recurrent metabolic decompensation. *Hum. Mutat.* 34:446–452. http://dx.doi.org/10.1002/humu.22257

Moore, C.B., D.T. Bergstralh, J.A. Duncan, Y. Lei, T.E. Morrison, A.G. Zimmermann, M.A. Accavitti-Loper, V.J. Madden, L. Sun, Z. Ye, et al. 2008. NLRX1 is a regulator of mitochondrial antiviral immunity. *Nature.* 451:573–577. http://dx.doi.org/10.1038/nature06501

Ott, M., V. Gogvadze, S. Orrenius, and B. Zhivotovsky. 2007. Mitochondria, oxidative stress and cell death. *Apoptosis.* 12:913–922. http://dx.doi.org/10.1007/s10495-007-0756-2

Pulskens, W.P., G.J. Teske, L.M. Butter, J.J. Roelofs, T. van der Poll, S. Florquin, and J.C. Leemans. 2008. Toll-like receptor-4 coordinates the innate immune response of the kidney to renal ischemia/reperfusion injury. *PLoS One.* 3:e3596. http://dx.doi.org/10.1371/journal.pone.0003596

Pulskens, W.P., E. Rampanelli, G.J. Teske, L.M. Butter, N. Claessen, I.K. Luirink, T. van der Poll, S. Florquin, and J.C. Leemans. 2010. TLR4 promotes fibrosis but attenuates tubular damage in progressive renal injury. *J. Am. Soc. Nephrol.* 21:1299–1308. http://dx.doi.org/10.1681/ASN.2009070722

Quirós, P.M., T. Langer, and C. López-Otín. 2015. New roles for mitochondrial proteases in health, ageing and disease. *Nat. Rev. Mol. Cell Biol.* 16:345–359. http://dx.doi.org/10.1038/nrm3984

Rebsamen, M., J. Vazquez, A. Tardivel, G. Guarda, J. Curran, and J. Tschopp. 2011. NLRX1/NOD5 deficiency does not affect MAVS signalling. *Cell Death Differ.* 18:1387. http://dx.doi.org/10.1038/cdd.2011.64

Singh, K., A. Poteryakhina, A. Zheltukhin, K. Bhatelia, P. Prajapati, L. Sripada, D. Tomar, R. Singh, A.K. Singh, P.M. Chumakov, and R. Singh. 2015. NLRX1 acts as tumor suppressor by regulating TNF-α induced apoptosis and metabolism in cancer cells. *Biochim. Biophys. Acta.* 1853:1073–1086. http://dx.doi.org/10.1016/j.bbamcr.2015.01.016

Soares, F., I. Tattoli, M.E. Wortzman, D. Arnoult, D.J. Philpott, and S.E. Girardin. 2013. NLRX1 does not inhibit MAVS-dependent antiviral signalling. *Innate Immun.* 19:438–448. http://dx.doi.org/10.1177/1753425912467383

Soares, F., I. Tattoli, M.A. Rahman, S.J. Robertson, A. Belcheva, D. Liu, C. Streutker, S. Winer, D.A. Winer, A. Martin, et al. 2014. The mitochondrial protein NLRX1 controls the balance between extrinsic and intrinsic apoptosis. *J. Biol. Chem.* 289:19317–19330. http://dx.doi.org/10.1074/jbc.M114.550111

Stokman, G., I. Stroo, N. Claessen, G.J. Teske, J.J. Weening, J.C. Leemans, and S. Florquin. 2010. Stem cell factor expression after renal ischemia promotes tubular epithelial survival. *PLoS One.* 5:e14386. http://dx.doi.org/10.1371/journal.pone.0014386

Stokman, G., Y. Qin, H.G. Genieser, F. Schwede, E. de Heer, J.L. Bos, I.M. Bajema, B. van de Water, and L.S. Price. 2011. Epac-Rap signaling reduces cellular stress and ischemia-induced kidney failure. *J. Am. Soc. Nephrol.* 22:859–872. http://dx.doi.org/10.1681/ASN.2010040423

Stokman, G., Y. Qin, T.H. Booij, S. Ramaiahgari, M. Lacombe, M.E. Dolman, K.M. van Dorenmalen, G.J. Teske, S. Florquin, F. Schwede, et al. 2014. Epac-Rap signaling reduces oxidative stress in the tubular epithelium. *J. Am. Soc. Nephrol.* 25:1474–1485. http://dx.doi.org/10.1681/ASN.2013070679

Susantitaphong, P., D.N. Cruz, J. Cerda, M. Abulfaraj, F. Alqahtani, I. Koulouridis, and B.L. Jaber. Acute Kidney Injury Advisory Group of the American Society of Nephrology. 2013. World incidence of AKI: a meta-analysis. *Clin. J. Am. Soc. Nephrol.* 8:1482–1493. http://dx.doi.org/10.2215/CJN.00710113

Wang, R., C.P. Dillon, L.Z. Shi, S. Milasta, R. Carter, D. Finkelstein, L.L. McCormick, P. Fitzgerald, H. Chi, J. Munger, and D.R. Green. 2011. The transcription factor Myc controls metabolic reprogramming upon T lymphocyte activation. *Immunity.* 35:871–882. http://dx.doi.org/10.1016/j.immuni.2011.09.021

Xia, X., J. Cui, H.Y. Wang, L. Zhu, S. Matsueda, Q. Wang, X. Yang, J. Hong, Z. Songyang, Z.J. Chen, and R.F. Wang. 2011. NLRX1 negatively regulates TLR-induced NF-κB signaling by targeting TRAF6 and IKK. *Immunity.* 34:843–853. http://dx.doi.org/10.1016/j.immuni.2011.02.022

Zuurbier, C.J., O. Eerbeek, and A.J. Meijer. 2005. Ischemic preconditioning, insulin, and morphine all cause hexokinase redistribution. *Am. J. Physiol. Heart Circ. Physiol.* 289:H496–H499. http://dx.doi.org/10.1152/ajpheart.01182.2004